Improved gold ion stripping at 0.1 and 10 GeV/nucleon for the Relativistic Heavy Ion Collider

P. Thieberger,* L. Ahrens, J. Alessi, J. Benjamin, M. Blaskiewicz, J. M. Brennan, K. Brown, C. Carlson, C. Gardner, W. Fischer, D. Gassner, J. Glenn, W. Mac Kay, G. Marr, T. Roser, K. Smith, L. Snydstrup, D. Steski, D. Trbojevic, N. Tsoupas, V. Zajic, and K. Zeno

C-A Department, Brookhaven National Laboratory, Upton, New York 11973, USA

(Received 25 September 2007; published 3 January 2008)

The four electron stripping stages leading to fully stripped gold ions in the Relativistic Heavy Ion Collider (RHIC) are briefly described. The third stripper, which removes 46 electrons from the Au^{31+} ions leading to heliumlike Au^{77+}, offers the greatest challenges in terms of energy loss and induced energy spread. These problems are described in detail as well as recent advances in the design and performance of this stripper. Measurements performed with several carbon and aluminum strippers show general agreement with a semiempirical model but small systematic deviations suggest that some model adjustments may be in order. The best performance is predicted and obtained with a combined carbon-aluminum foil system. Measurements showing the enhanced performance in the alternating gradient synchrotron are described. The stripper that removes the last two electrons has also been improved and the results of relevant calculations and measurements are presented.

DOI: 10.1103/PhysRevSTAB.11.011001 PACS numbers: 29.20.db, 29.20.dk

I. INTRODUCTION

Electronic charge-exchange processes are of fundamental importance for the design and performance of heavy ion accelerators and, in particular, for an accelerator complex such as the Relativistic Heavy Ion Collider (RHIC). On the one hand, before final acceleration and storage, all the electrons need to be removed in as few stripping steps as possible that need to be as efficient as possible while at the same time minimizing adverse effects on beam quality. On the other hand, residual gas induced charge-exchange beam losses need to be understood and minimized for the various stages of beam acceleration, transport, and storage. Experiments performed at the Bevalac in the 1980s [1–10] served to establish some of the RHIC design parameters and to improve the theoretical understanding of charge-exchange processes when relativistic heavy ions traverse solids and gases [11–17]. This improved understanding and comparison to experiments, also based on important measurements performed at GSI [18–21], has more recently been reviewed [22] and made easily accessible in the form of semiempirical computer codes GLOBAL and CHARGE incorporated in the LISE++ code [23,24]. Stripping efficiency measurements and charge-exchange studies for gold beams were performed at the BNL booster and the alternating gradient synchrotron (AGS) by Roser [25] and by Roser, Ahrens, and Hseuh [26]. Limitations of charge exchanges processes for the booster operation were recently simulated by Smolyakov, Fischer, Omet, and Spiller [27].

In the following sections we briefly describe the four gold stripping stages in the RHIC complex and we then concentrate on the third stripper where by far the largest relative energy loss takes place ($\sim 4\%$) and which offers the largest challenge in terms of minimizing adverse effects on longitudinal emittance. We show that microscopic nonuniformity of the graphite stripper used so far was responsible for significant beam energy spread in the AGS. We then study the possibility of using other materials by using the GLOBAL code, and find that a combination of aluminum and carbon foils offers a slightly enhanced stripping efficiency and an energy loss that is only $2/3$ as large as before. We then describe the implementation of this combined Al-C stripper by using commercial aluminum foil and newly available films of glassy or vitreous carbon, thus virtually eliminating the energy spread due to thickness nonuniformity. We describe results of measurements performed in the AGS showing enhanced performance and we discuss the impact on the new bunch merge scheme [28] and on the overall RHIC performance. Finally, for the last stripper we discuss the advantages of making it thinner and of using a material of higher atomic number.

The RHIC facility gold stripping scheme

The sequence of heavy ion acceleration and stripping stages for RHIC gold injection have been often described before (see e.g. [28,29]) and are schematically shown in Fig. 1. The accelerators involved are either one of two 14 MV available Tandem Van de Graaff accelerators (MP6 and MP7) and two synchrotrons: the fast cycling AGS booster and the AGS. The first stripper is located in the 14 MV Tandem terminal and is called the terminal stripper and the second one is the object stripper located at the object point at the beginning of the beam transport from the Tandem to the booster (the so-called TTB line which is 800 m long). The last two strippers are between the booster and the AGS, in the so-called BTA line, and between the

*PT@BNL.GOV

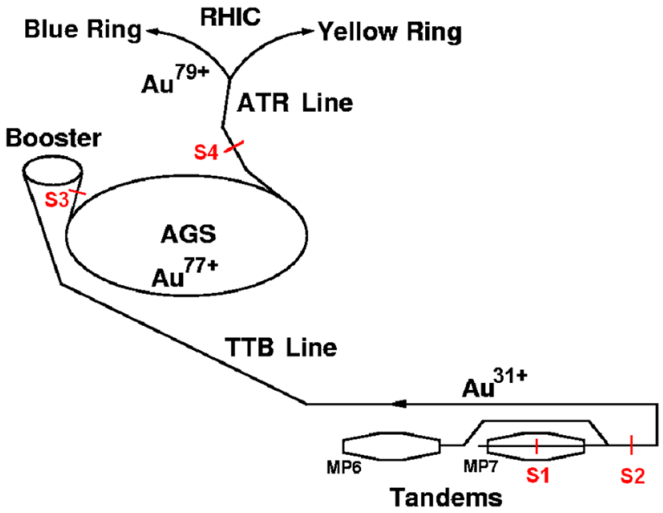

FIG. 1. (Color) Schematic diagram of the chain of RHIC injectors where the electron stripping foils have been labeled S1 through S4 corresponding to the strippers listed in the same order in Table I.

AGS and RHIC, in the so-called ATR line, and they adopt the respective names of these transport lines.

Table I summarizes the material and thickness of these four strippers, the gold beam energies, and energy losses at each of them as well as the resulting selected charge state and its relative abundance. This was the situation before the improvement of the BTA and ATR strippers described later.

The energy loss values for the terminal and object strippers are rough estimates obtained by using the TRIM code [30]. The BTA stripper energy loss value of 3.74% is accurately obtained from booster and AGS frequency measurements and can be compared to the 4.2% value obtained from TRIM. The difference is probably due to the fact that the ion transitions from charge 31^+ to charge 77^+ while traversing the foil and its average charge state is thus significantly lower than the equilibrium charge state. The energy loss in the ATR stripper is measured by comparing magnetic deflections. The measured value ($0.35\% \pm 0.05\%$) is in agreement with the 0.33% estimate from TRIM.

The thicknesses of the graphite strippers have been optimized over the years to obtain near to maximum yields with the smallest possible thicknesses and energy losses. We see from Table I that the relative energy loss in the BTA stripper (3.7%) is by far the largest. This causes the following bunch-phase mismatch problems between the booster and the AGS [28,29].

The orbit length in the booster is $\frac{1}{4}$ of the orbit length in the AGS, and the orbital frequencies ratio would therefore need to be 4 to 1 in order to place each injected bunch at the synchronous energy of the corresponding AGS bucket. However, due to the energy loss in the BTA stripper, those bunches would then have a velocity that is about 1.6% lower than the synchronous velocity of the AGS buckets. One then increases the booster frequency by $\sim$1.6% to compensate, which allows all of the six bunches to be perfectly matched in energy (velocity), but the higher booster frequency implies that the time interval between the bunches is 1.6% less than the spacing between adjacent AGS buckets and consequently only one bunch can have the correct phase with respect the AGS bucket. This problem could be reduced if the stripper could be made thinner without sacrificing stripping efficiency. As discussed later, a reduction from 1.62% to 1.08% was achieved.

Because of the relatively large energy loss, another important concern is the thickness uniformity of this stripper, which needs to be very good to avoid introducing excessive energy spreads. This subject is discussed in the next section.

II. THE NONUNIFORMITY PROBLEM WITH THE BTA GRAPHITE STRIPPER

Considerable gold beam energy spread following the BTA stripper was observed during early booster-AGS operation and this energy spread was initially attributed to the so-called energy straggling, an unavoidable energy loss fluctuation inherent to the statistical nature of the collisions that occur with the electrons and nuclei in the solid. However, by using estimates from the semiempirical code TRIM [30], it was soon realized that the observed energy spread was much larger than could be expected. It was then suspected that an important contribution to the energy spread must originate from stripper foil nonuniformities. This suspicion was confirmed in extensive measurements performed by studying the energy loss of various low energy monoenergetic beams at the Tandem Van de Graaff facility incident on the same material used in the fabrication of the BTA strippers.

TABLE I. Gold stripping characteristics before the present stripper improvements.

Stripper name	Material	Surface density (g/cm^2)	Incident energy (MeV)	Energy loss (MeV)	Energy loss (%)	Selected charge (Q)	Yield of Q (%)
Terminal	Graphite	2×10^{-6}	14	0.044	0.31	12	20
Object	Graphite	16×10^{-6}	182	1.52	0.84	31[a]	15
BTA	Graphite	24.2×10^{-3}	1.97×10^4	736 ± 2	3.74 ± 0.01	77	63
ATR	Al_2O_3	522×10^{-3}	1.97×10^6	6900 ± 100	0.35 ± 0.05	79	99.99

[a]In previous years, charge 32 was selected here.

Energy spectra of low energy protons or other ions are obtained using a silicon detector, and collecting the data in a multichannel pulse-height analyzer before and after inserting foils of various materials. One of these foils was the 0.005 in. (24.2 mg/cm^2) thick graphite sheet routinely used for stripping the gold ions in the BTA line [31]. The foil can be scanned by displacing it in small steps across the horizontal ~1 mm diameter beam, both in the vertical as well as in the horizontal direction to detect macroscopic thickness variations. Figure 2 shows the result of one of these measurements where a mica foil was compared to the 0.005 in. graphite material.

In this example, we see a much larger energy spread for the graphite as compared to the mica. The combined contribution of the beam energy spread and detector resolution is very small as can be seen by the width of the ''no absorber'' peak. Scanning the beam across the graphite foil resulted in negligible thickness variations. The conclusion is that there are significant nonuniformities on a scale much smaller than 1 mm, which are probably microscopic, and due to porosity associated with the microcrystalline nature of the material.

We used data like these to calculate the microscopic nonuniformity of various stripper materials by taking into account the contribution to the widths of the peaks due to energy loss straggling calculated by using TRIM. In addition, the sample is always scanned across the beam to determine macroscopic thickness variations. In the case shown in Fig. 2, the width of the ''mica'' peak is almost exclusively due to straggling while the ''carbon'' peak width is dominated by the graphite microscopic nonuniformity. Once the nonuniformity is known for a given foil, its impact on the beam energy spread at AGS injection can be calculated when that foil is used as BTA stripper by using the TRIM code [30] for energy loss calculations. The other contributors to that energy spread are the energy spread of the incident beam from the booster and energy loss straggling.

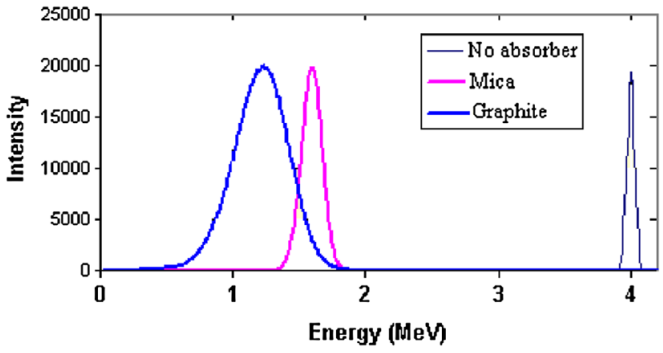

FIG. 2. (Color) Proton energy spectra showing the full energy, 4 MeV, peak, and two lower energy peaks obtained by inserting a 0.005 in. graphite plate made of the same material used for the BTA stripper and a similar thickness uniform mica plate. The proton energy loss measures the thickness of the material traversed. The width of the mica peak is almost fully accounted for by the calculated [30] proton energy loss straggling plus a small contribution from the detector resolution. The extra width of the ''graphite'' peak is due to microscopical nonuniformity of the material, presumably due to its porosity.

Figure 3 shows these contributions for five different strippers as well as the resulting total expected gold energy spread after the BTA stripper. We see that for this beam the straggling contributions are negligible and that the nonuniformity effect predominates in the case of the graphite strippers. We also show the corresponding energy spread measurements performed in the AGS by measuring the debunching rate in each case [32]. We find fairly good agreement for most strippers except in the fused silica case where measurement difficulties were encountered and we were unable to repeat the measurement.

We see from Fig. 3 that in principle a considerable reduction in the energy spread is possible. In particular, for the graphite strippers, almost the entire energy spread is due to nonuniformity. The fused silica foil was used for some time, even though the charge 77^+ yield was somewhat smaller than for the 0.005 in. (24.2 mg/cm^2) thick graphite stripper. The energy spread was indeed much reduced but after some time the energy spread started to increase, and it was later found that radiation damage had deformed the foil. The yield for the mica stripper was somewhat smaller than for the fused silica, and it was much smaller for the titanium stripper. Intensity is a critical parameter for RHIC gold operation.

This was the situation until recently. The best yield of heliumlike gold was obtained with graphite strippers, which had however the disadvantage of introducing a large energy loss and excessive energy spread. The problem was understood and it was clear that there was considerable

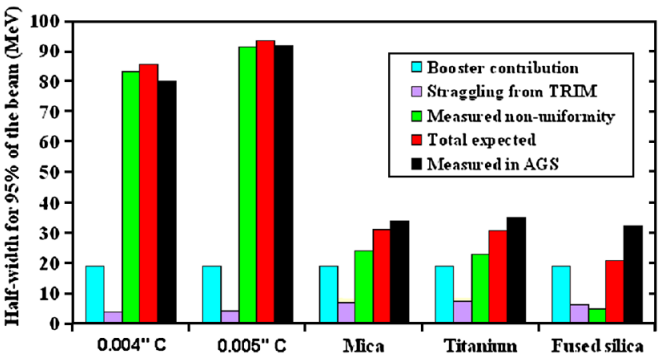

FIG. 3. (Color) Expected and measured gold beam energy spreads at AGS injection obtained with five different BTA stripper materials. The expected values are computed by adding in quadrature the contributions due to the energy spread of the beam from the booster, a negligible contribution from energy loss straggling and measured thickness nonuniformities. The nonuniformity contribution dominates by far for the graphite strippers. The measured energy spreads are obtained by measuring debunching rates in the AGS [32]. Measurement difficulties for the fused silica case may explain the relatively large discrepancy with the expected value.

room for improvement, but there were no good practical alternatives. Since then two events made further progress possible as described in the next sections. The new codes "GLOBAL" and "CHARGE" [22–24] were developed that make it easy to estimate charge-state yields for different materials and over a wide range of energies and ion species, and nonporous so-called glassy or vitreous carbon became available in thin sheets [33].

A. GLOBAL model estimates for different materials

In the 1980s, several experiments [1–10] were conducted at the Bevalac to study heavy ion charge-exchange cross sections and stripping efficiencies for ion kinetic energies up to 1 GeV/nucleon. The primary purpose of these measurements was to establish design parameters for RHIC and the RHIC injectors and beam transfer lines in terms of vacuum requirements and strippers to be used. The theorists Meyerhoff and Anholt participated actively in these experiments and then used the results to develop a better understanding and semiempirical models [11–17] that provide good fits to the data and that allow some reasonable degree of extrapolation. Later, additional important experimental and theoretical work took place at GSI [18–21]. More recently these models were integrated into the user friendly codes GLOBAL and CHARGE [22,23] that are now part of the LISE++ software package [24].

We show the results of GLOBAL estimates for 100 MeV/nucleon charge 77^+ yields for aluminum carbon and beryllium strippers in Fig. 4. Rather than plotting the yields as a function of stripper thickness, we plot them as a function of energy at the exit of the foil (which in turn is a function of the thickness). In this way the quantities of interest for optimizing the performance are clearly visible.

It should be noted that, for these estimates, the GLOBAL program restriction to ions with at most 28 electrons precludes using as input the real number of electrons present on a charge 31^+ gold ion which are 48. However, these more loosely bound extra 20 electrons will come off very quickly and will barely affect the result [34]. We estimate that the maximum yields shown in Fig. 4 may be reduced by up to 1% due to this effect. The extrapolation that leads us to this estimate is shown in Fig. 5. Rather than making an uncertain correction, we show the results as calculated with the maximum allowed number of electrons on the incident ions.

The square red dot on the carbon curve in Fig. 4 corresponds to the thickness of the 0.005 in. stripper that was the standard so far. The first comment we can make is that the empirically chosen thickness is very close to the optimal thickness predicted by GLOBAL. We also see that lighter (Be) and heavier (Al) strippers do not perform as well as carbon, again confirming what we have learned through experience. Increasing the thickness of the aluminum stripper causes the charge 77^+ to rise more quickly than is the case for carbon, but the maximum yield is lower. Beryllium, on the other hand, may eventually reach a similar yield, but at an energy loss that is much larger.

Combining the fast-rise advantage of aluminum with the best ultimate yield of carbon seems to be the best solution. GLOBAL calculations for such a combined stripper were performed and the chosen operating point is indicated by

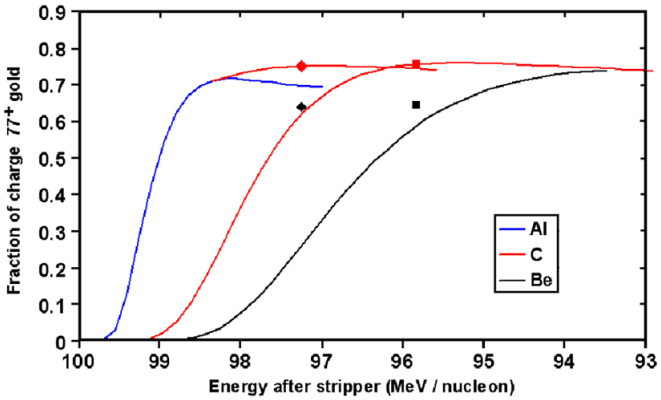

FIG. 4. (Color) Estimated heliumlike gold yields in the BTA stripper for 100 MeV/nucleon incident gold ions as a function of the energy after the stripper, for increasing stripper thicknesses. These estimates were calculated with the GLOBAL program [24] for aluminum, carbon, and beryllium strippers and for a special combination of aluminum and carbon foils that takes advantage both of the rapid rise of the "Al" yield and of the slightly larger ultimate "C" yield. The red square dot indicates the prediction for the old BTA graphite stripper while the red diamond-shaped dot corresponds to the new aluminum-glassy carbon stripper. The actual measured values are lower as indicated by the black dots.

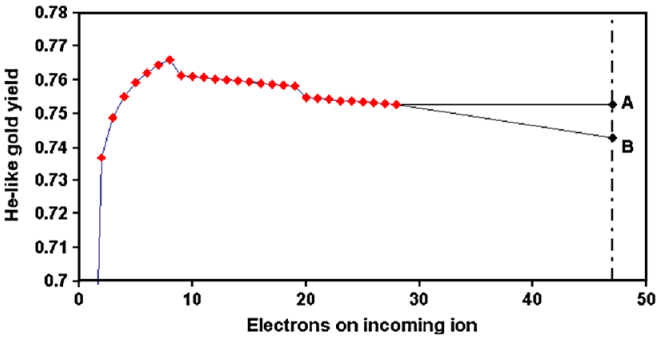

FIG. 5. (Color) GLOBAL program results for 100 MeV/nucleon gold ions with 2 through 28 electrons incident on a 23.1 mg/cm^2 graphite foil. These results are used to estimate, through extrapolation, the He-like gold yield for incident Au^{31+}, which has 48 electrons. While this latter case can at present not be calculated with GLOBAL, the additional 20 electrons are expected to have little influence on the result [34] as they are more loosely bound and come off almost immediately as the ion starts penetrating the foil. Points A and B represent, respectively, two extreme extrapolations where either no further change takes place, or the average downward slope of the curve (which is expected to level off) does not change. The yield difference between these two extreme cases is only ~1%.

the red diamond-shaped dot in Fig. 4. We see that, as expected, the yield can be the same or slightly larger than for carbon, but due to the faster initial rise in aluminum, the overall energy loss is about 1/3 less. Furthermore, aluminum foils do not have the porosity problem of the graphite strippers, and the thinner carbon foil required here was made out of a nonporous carbon material as described in the next section.

B. The combined aluminum-vitreous carbon foil system

Nonporous vitreous or glassy carbon is a form of carbon that has been known for a long time, but only recently has it become available in thin sheets [33]. Fortunately, one of the standard thicknesses was appropriate for this application and is the one used to generate the estimate in Fig. 4. While aluminum foils of any thickness can be easily rolled, this was not necessary since commercial ''heavy duty'' Reynolds Wrap® was found to have the right thickness. The thicknesses of both of these materials were checked by careful weighing of well-measured square samples. The surface densities of the aluminum and glassy carbon foils are, respectively, 6.4 ± 0.1 and 9.2 ± 0.2 mg/cm^2.

The vitreous carbon foil, which is rather brittle was laser cut to the right shape as shown in Fig. 6 and then mounted on the support (also shown) with a screwed-on clamp that was left somewhat loose to allow for differential expansion during baking. The aluminum foil was clamped to the other side of the support leaving a 1.5 mm wide gap between both foils for pumping. When mounting this assembly in the stripper housing, it is important that the beam enters through the aluminum side and exits from the carbon side; otherwise the results would be disappointing.

After this stripper was installed in the BTA line, a series of charge-state distribution measurements were performed as described in the next section.

C. Measured charge-state distributions and comparisons with the semiempirical predictions

Charge-state distribution measurements were performed by using regular beam transport elements and instrumentation available in the BTA line. A multiwire beam profile monitor (''harp'') [35] was used to normalize the incoming beam, and a second such beam profile monitor located after a dipole magnet was used to measure the individual charge-state intensities.

Sometimes two consecutive charge states were observed simultaneously as shown in Fig. 7, but most often single charge states, adjusted so as to fall close to the center of the harp, were recorded. The red points indicate the channels that were used to obtain the areas of the peaks. Normalizing these areas with the intensity simultaneously recorded with the first harp, and then renormalizing the sum of all the charge states that contain measurable intensities to 100%, we obtain the charge-state distributions shown in Fig. 8 for the seven strippers present in the foil changer.

In Fig. 8 we show the comparisons between measured and predicted charge-state distributions for the seven stripper foils available in the BTA foil changer during the 2007

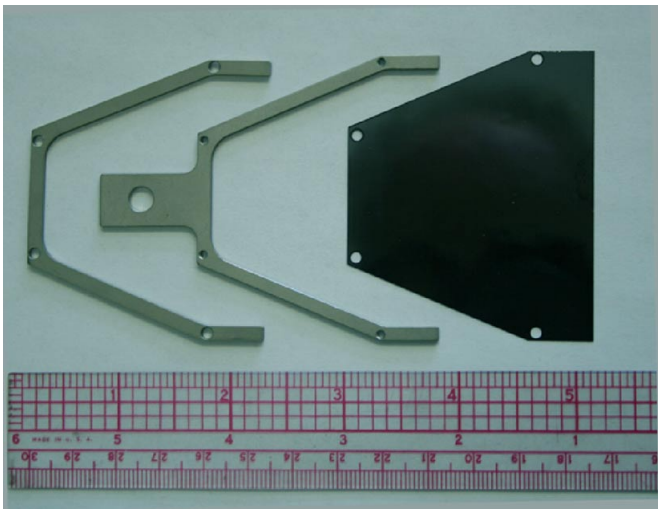

FIG. 6. (Color) Photograph of the glassy carbon stripper and foil holder. The clamp shown to the left attaches with pairs of countertightened nuts to studs threaded through the foil holder holes so as to avoid clamping the stripper too tightly to allow for differential expansion during baking. A second clamp (not shown) is used to attach the aluminum foil to the other side of the holder.

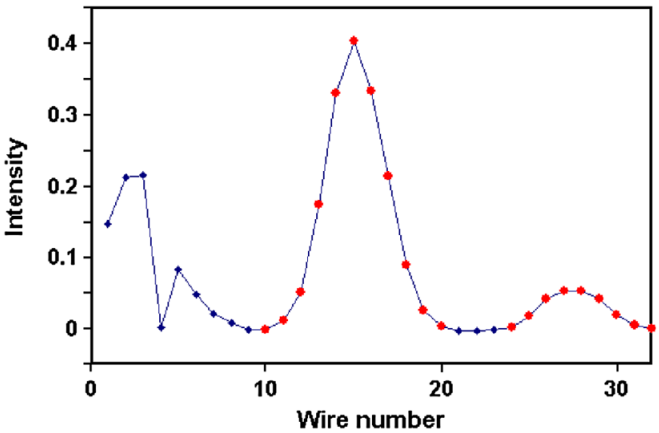

FIG. 7. (Color) Example of a gold beam profile obtained after the BTA stripper and following a dipole magnet that separates the charge states. The central peak in this case is charge 77^+, or heliumlike gold, while the one to the left is 76^+ and the one to the right 78^+ (hydrogenlike gold). The areas under these peaks, normalized to similar profiles measured before the stripper, are used to calculate the charge-state distributions. Often only the central peak is usable (note, e.g., the bad No. 4 wire), and the beam transport is retuned from charge to charge. Red dots indicate the values added to obtain the peak areas while adjacent blue dots were used to estimate the background subtraction.

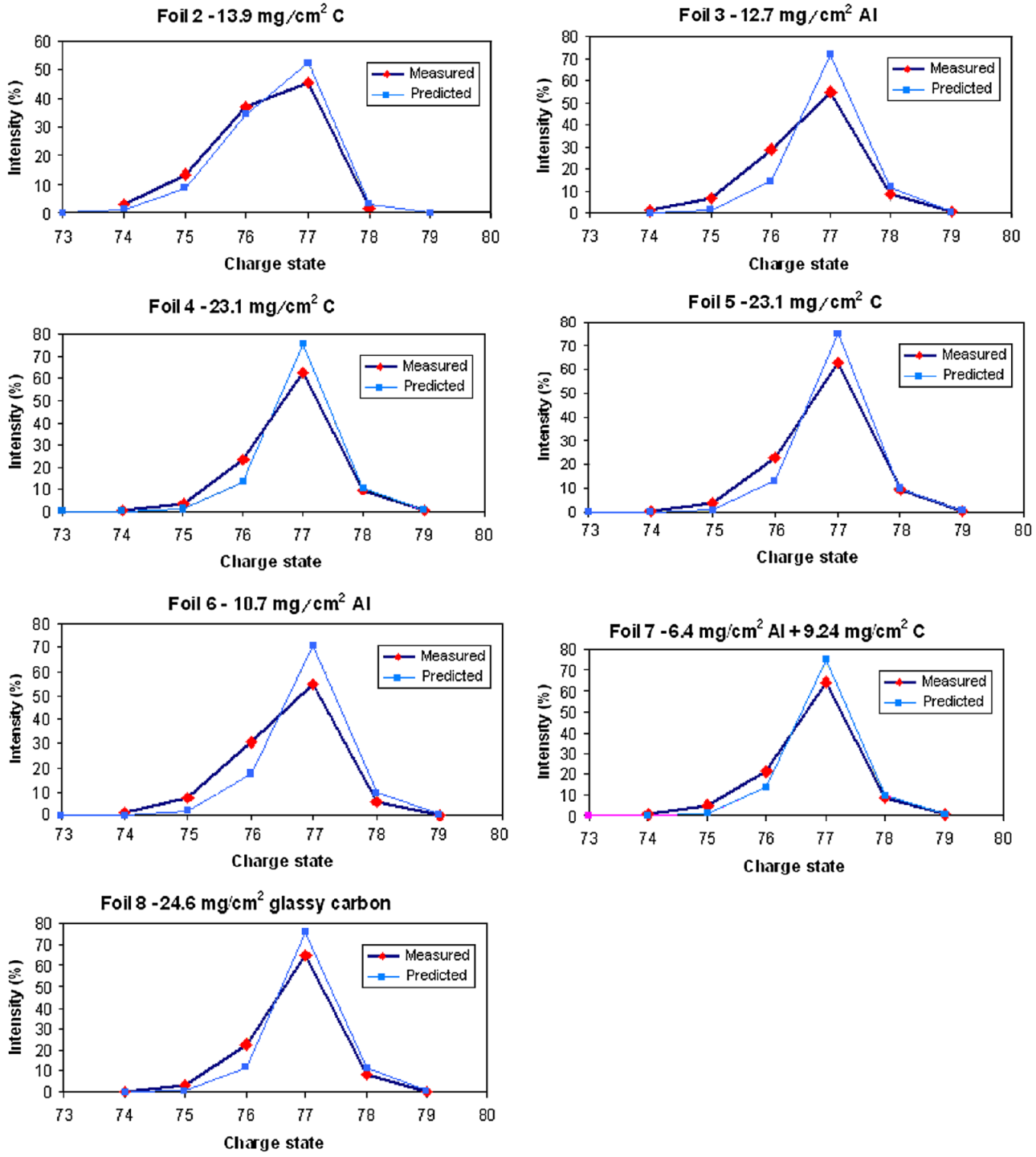

FIG. 8. (Color) Measured and predicted [24] 100 MeV/nucleon gold charge-state distributions for the seven stripper foils installed in the BTA stripper box during the 2007 run.

run. We see that shapes predicted by GLOBAL are very similar to the measured ones, but in most cases the measured distributions are somewhat wider yielding smaller charge 77^+ yields. The results for charge 77^+ are summarized in Fig. 9.

The pattern of measured charge 77^+ gold yields is very similar to the pattern of predicted values, but the measured values are systematically smaller. These differences are significantly larger for the two aluminum strippers. As mentioned above, only a small part of these differences may be attributable to the GLOBAL code limitation of having a maximum of 28 electrons on the incoming ion. Since our measurements fall outside of the energy range of previous experiments, these systematic deviations may

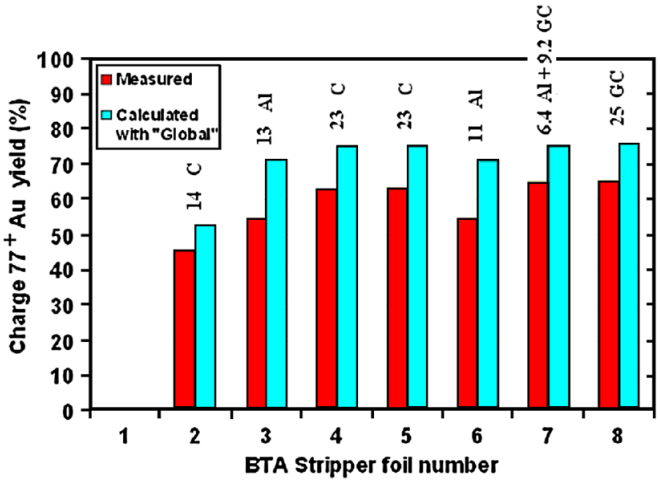

FIG. 9. (Color) Heliumlike 100 MeV/nucleon gold yields (in red) measured with the seven strippers installed in the BTA line for the 2007 RHIC run, and corresponding estimated yields (in blue) calculated with the GLOBAL program. The numbers in the labels mean mg/cm^2. The C for foils 2, 4, and 5 stands for graphite, while "GC" for foils 7 and 8 means glassy carbon. Note the relatively small but systematic deviations and the fact that these deviations are significantly larger for the two cases where the beam exits from aluminum (foils No. 3 and No. 6).

indicate the need for adjusting some parameters, or otherwise refining the model.

D. Improved performance in the AGS

Four transfers from the booster to the AGS, each containing 6 bunches, occur in an AGS cycle. Each of these transfers is separated by the length of the booster acceleration cycle, which is 200 ms. So, beam from the first booster transfer must survive across a 600 ms injection magnetic porch. The 24 bunches are then merged into 4 bunches and accelerated.

As we saw before, the charge 77^+ yield of the new combined aluminum + glassy carbon BTA stripper is 1% or 2% better than before, and the energy loss is reduced to about 2/3 of its previous value. This last change reduces the phase error between the newly injected bunches and the AGS rf buckets [28,29]. But it is the reduction in energy spread of the incoming bunches due to the improved foil uniformity that is the major reason for the improvement in longitudinal emittance. With the old foil, the incoming bunches were too large in energy spread to be caught smoothly by the AGS rf. There was not sufficient voltage available and the bunches instead pin wheeled around in the buckets ultimately filamenting to be even larger in longitudinal phase space. The bunch energy spread with the new foil is easily matched with the AGS rf system and only the phase mismatch remains as a cause for dilution. This effect, which was subtle with the old foil and is smaller now than then, is nevertheless now the dominant cause for dilution. The situation is much improved.

As explained in detail in the Fig. 10 caption, we obtain a good picture of the early behavior of six AGS bunches as they are injected from the AGS booster, which allows us to compare the performance with the old BTA stripper (a) with the new one (b). The bunch shapes are recorded by a wall monitor detector and displaced vertically in the display so as to have turn No. 1 at the bottom and turn No. ~80 at the top.

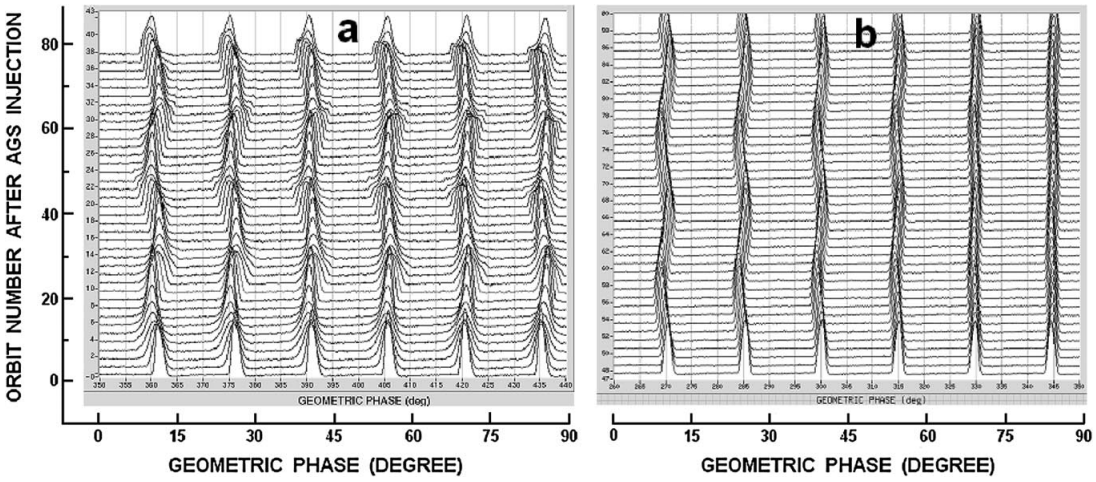

FIG. 10. Gold bunches at AGS injection, as measured using a wall monitor detector and displayed as "mountain ranges" for the previous run (a) using the nonuniform graphite BTA stripper and (b) with the new aluminum-glassy carbon improved BTA stripper used during the 2007 run. The horizontal axis is time, actually plotted as phase, where 360 degrees correspond to a full AGS turn (6.3 μs). The AGS harmonic is 24, so the nominal bunch spacing is 15 degrees (263 ns), and one AGS booster cycle fills $\frac{1}{4}$ of the AGS ring. The vertical scale measures instantaneous current amplitude (arbitrary scale) and the curves are vertically displaced so as to show the first turn at the bottom and, in succession, every second turn going up. The improvement is due both to the better uniformity of the new BTA stripper and to the reduced kinetic energy loss (2.45% as compared to 3.74%).

Comparing the curves (a) and (b) in Fig. 10 we see that the first turns (at the bottom) look quite similar. The relative vertical (intensity) scaling between (a) and (b) is arbitrary, but the base widths have the same scale and are about the same. However, the evolution in the two cases is very different and reflects the foil properties discussed before. Both show evolution over a little more than two synchrotron oscillations. In (a) the bunch is ''mismatched'' to the rf bucket, pin wheeling—the projection growing fatter and then thinner—twice each synchrotron period. The rf voltage in the AGS is not high enough and cannot be made high enough to remove this behavior.

In addition, the center of mass of a bunch moves back and forth over successive turns due to the phase error resulting from the energy loss in the foil [28,29]. In (b) there is no visible pin wheeling. The rf voltage can be—and is—adjusted to remove this mismatch. The center of mass motion is then very obvious. This data (b) actually overemphasizes this attribute since the last bunch was adjusted to have roughly the correct phase. For normal running, the average bunch phase relative to the rf is adjusted to ''split the difference'' in such a way that the two central bunches (Nos. 3 and 4) show the smallest oscillation. The worst case then corresponds to the first and last bunch which during normal injection are adjusted to show equal oscillations and look similar to the central bunches shown in Fig. 10(b) for the present test. This remaining phase error is not corrected and is still large—though small compared with every bunch in (a)—resulting in the phase space occupied increasing by a factor ~ 1.7.

Compared to the previous run where the 0.005 in.-thick graphite BTA stripper was used, the longitudinal emittance growth due to the foil is reduced from a factor of 4 to a factor 1.8. While we were unable to do detailed foil uniformity studies with the new aluminum-glassy carbon stripper, we do get an overall energy spread reduction that is almost identical to the one obtained before with the most uniform older strippers (see Fig. 3), namely, a reduction in half width from 92 ± 1 MeV obtained with the old graphite stripper to about 32.5 ± 1 MeV now. As before, with microscopically homogeneous strippers surface irregularities remain a source of energy loss fluctuations. Had we used the old graphite material [31] for the carbon component of the new striper, we estimate that its contribution to the energy spread would have been ~ 55 MeV since the statistical thickness fluctuations due to porosity are expected to scale with the square root of the thickness. At extraction, the longitudinal emittance is reduced from 0.40 eV-s/nucleon before to 0.23 eV-s/nucleon at present [28].

The overall beam transfer efficiency from the booster to the AGS has improved too, from about 53% when using the old 0.005 in. graphite stripper to about 58% with the new aluminum + glassy carbon stripper. Since the charge 77^+ yield increased by only $\sim 2\%$ (from 63% to 65%), there must have been a reduction in the other losses that occur during the injection process. This additional improvement is likely to be associated with the beam's smaller longitudinal emittance in the AGS which generally results in a beam that is smaller horizontally and therefore less likely to scrape on the aperture. It may also be due, in part, to the beam's smaller momentum spread as it is transported through the BTA line and injected into the AGS.

Another mechanism suspected of contributing to the observed losses across the long injection porch is the betatron tune spread of the beam in the AGS. As beam particles in the AGS circulate for the 600 ms required to complete injection, they undergo synchrotron oscillations which cause the betatron tunes of individual particles to change due to nonzero chromaticity. The range of betatron tunes over which these particles move is larger for a beam with a larger longitudinal emittance. This can cause particles to pass through resonances that occur at particular betatron tunes and which may cause particles to be lost. With a smaller longitudinal emittance, the tunes of the particles can be better controlled, and these resonances more successfully avoided.

Thus we conclude that the 5% improvement in the transfer efficiency observed during the most recent run is due both the improved 77^+ yield (1%–2%), and to the improved characteristics of the 77^+ beam which have been described above.

III. IMPROVED ATR STRIPPER

This is the fourth and last stripping stage. One of the 1 mm-thick aluminum oxide beam profile monitor flags [36] positioned at 45° to the beam (522 mg/cm^2 effective surface density) was used since operations started as the stripper responsible for removing the last two electrons from the gold ions before injection in RHIC. As can be seen from Table I, the stripping efficiency was good and the energy loss was only $\sim 0.3\%$ of the beam energy so that no large effects due to energy straggling or foil nonuniformity were expected or observed. It was however realized that this stripper was thicker than necessary, and that it caused a significant beam intensity loss (about 4%) due to nuclear fragmentation, and also some non-negligible angular scattering affecting the transverse emittance of the beam. The beam loss was not only wasteful, but it caused significant radiation levels and potential soil activation problems in the vicinity of this stripper.

Different possible materials were considered for a new ATR stripper by obtaining stripping efficiency predictions [24] and energy loss and energy loss straggling estimates [30]. Figures 11 and 12 illustrate some of the estimates used for these comparisons for two of the candidate materials, aluminum and tungsten, respectively.

We see from Figs. 11 and 12 that the aluminum stripper needs to be ~ 5 times thicker than tungsten in terms of surface density (mg/cm^2). The fact that the energy loss is

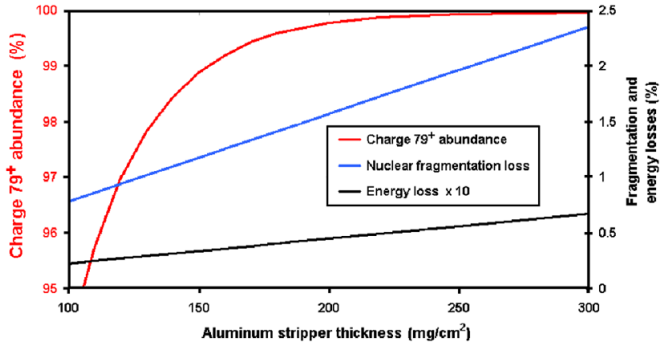

FIG. 11. (Color) Calculated stripping efficiency, energy loss, and intensity loss due to nuclear fragmentation for a 10 GeV/nucleon gold beam incident on an aluminum stripper as a function of stripper thickness.

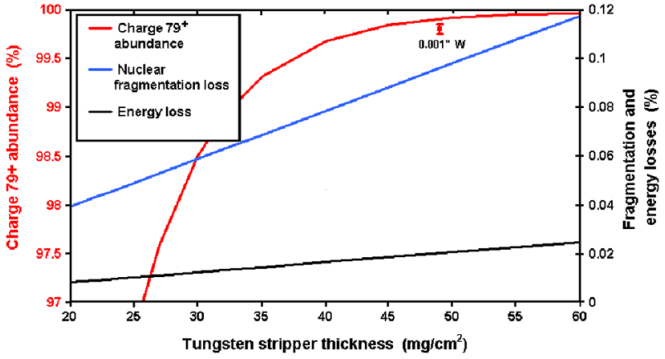

FIG. 12. (Color) Calculated stripping efficiency, energy loss, and intensity loss due to nuclear fragmentation for a 10 GeV/nucleon gold beam incident on a tungsten stripper as a function of stripper thickness. Note that both the horizontal scale for stripper thickness as well as the right vertical scale for energy and intensity losses differ from the ones used in Fig. 11. The data point labeled 0.001 in. thick W (48.9 mg/cm^2 surface density) was obtained by measuring beam intensity lost to charge states 78^+ and 77^+ (see text).

larger for aluminum is not very relevant because it is still very small ($\sim 0.06\%$ for a stripper of appropriate thickness), but nuclear fragmentation losses are much larger (2% versus 0.1% for tungsten). While better than the $\sim$4% losses we had before, tungsten is clearly preferable. Consequently, a 0.001 in. thick (48.9 mg/cm^2) tungsten stripper was installed and is now being used.

Measurements were performed of the relative intensities of charge components 77^+, 78^+, and 79^+ by using an existing beam profile monitoring system that consists of cameras viewing, digitizing, and recording the beam spots produced on fluorescent screens [36]. The relevant charge states are selected with the first beam transport dipole following the stripper, and calibrated neutral density filters are used to select a light intensity appropriate for the dynamic range of the camera. The results show that the efficiencies for obtaining fully stripped gold ions are $99.8\% \pm 0.05\%$ for the 48.9 mg/cm^2 tungsten foil and $\geqq 99.99\%$ for the old 522 mg/cm^2 Al_2O_3 stripper. The losses due to incomplete stripping are negligible in both cases. For the W stripper this loss is slightly larger than expected (see Fig. 12).

We finally consider the contributions of the old and the new ATR strippers to the angular spread of the beam. For that purpose we run SRIM [30] to simulate the transport of 50 000 9.1 GeV/nucleon and 9.6 GeV/nucleon gold ions through each stripper, we perform a statistical analysis of the results using an Excel spreadsheet, and we then extrapolate the results to 10 GeV/nucleon. The reason for having to do this slight extrapolation is that the program is not reliable close to its energy maximum of 10 GeV/nucleon. Even so, the results can only be considered as rough estimates due to the lack of experimental verification at these energies. The results of these calculations are shown in Table II. While the new stripper has an areal density about one-tenth of the old one, the estimated angular spread is reduced only by approximately a factor two because of the large atomic number of tungsten.

A first measurement of the scattering due to the Al_2O_3 stripper gave an rms angular spread of 100 ± 15 micro radians. While the TRIM estimates close to 10 GeV/nucleon are not very reliable, this large discrepancy is nevertheless somewhat surprising. This measurement will be repeated and extended to also include the tungsten stripper.

TABLE II. Estimated multiple scattering contributions to the angular spreads of gold beams in the old and the new ATR strippers, measured stripping efficiencies, and calculated nuclear fragmentation losses.

ATR stripper	Effective surface density (mg/cm^2)	Rms angular spread due to the stripper (microradians)	Measured charge 79^+ stripping efficiency (%)	Calculated nuclear fragmentation losses (%)
Al_2O_3 (old)	522	29.7	≥ 99.99	5.7[a]
W (new)	48.9	14.2	99.8 ± 0.05	0.1

[a]The measured loss due to fragmentation is $4\% \pm 0.5\%$, indicating that the effective nuclear radius, R, used in the fragmentation calculations may be $\sim$16% too large. The expression used was $R = R_0 \times A^{1/3}$, with $R_0 = 1.2$ fm.

IV. BEAM EFFECTS ON THE STRIPPERS

Radiation damage, heating effects, deposition of cracked hydrocarbons, and sputtering are all factors that can affect the performance and lifetime of stripper foils. The last two effects are only relevant for the very thin (few $\mu g/cm^2$) foils used in Tandem Van de Graaff accelerators. There is ample experience with stripper foil lifetimes in Tandems (see e.g. [37]), and the recent use of laser ablation foils [38] in MP7 has been a major improvement.

The BTA graphite strippers used before had a long lifetime without clear evidence of deterioration. However, the new aluminum-glassy carbon combination seems to be affected significantly by the gold beam. While no performance degradation was observed, visual inspection of this stripper indicates that the useful lifetime will be shorter than for the graphite strippers. Figure 13 is a composite of pictures taken from the aluminum and form the carbon side, where the second one has been flipped horizontally to facilitate comparison. The observed patterns are not well understood, but signs of discoloration and deformation are evident on both sides. Deformation is particularly worrisome for this stripper because at some point it will lead to significant variations in effective thickness. An estimated total of 5×10^{15} gold ions traversed this stripper, the rms beam horizontal and vertical beam dimensions were both about 4 mm, and the maximum intensity was 3.3×10^9 ions per booster cycle. Two new identical strippers have now been installed, and their performance will be carefully compared with the performance of the used one.

In order to extend the operational lifetime, in addition to mounting multiple strippers, one could also consider modifying the foil changer mechanism so as to allow moving the foil across the beam as is being done with some of the Tandem strippers [37]. Another countermeasure that will be adopted in the future is to evaporate a thin graphite film onto both sides of the aluminum foil to improve thermal radiation emittance and minimize any possible effects of heating, both for the carbon and for the aluminum.

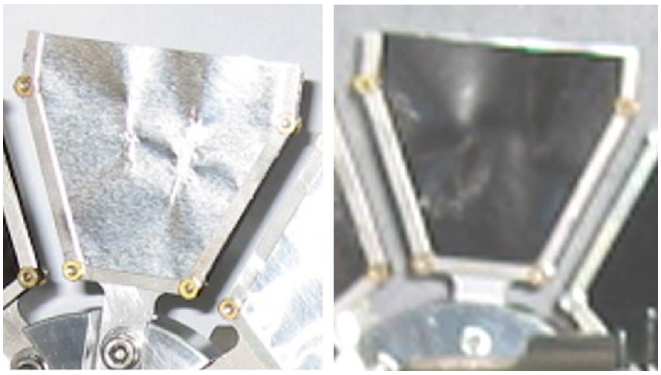

FIG. 13. (Color) Front and back of the aluminum-glassy carbon BTA stripper after the 2007 gold run. The picture of the carbon side has been horizontally flipped to aid in the comparison.

The new tungsten ATR stripper has not been examined, but large effects are not likely there because of the much smaller number of ions traversing this foil, the smaller value of dE/dx and the refractory properties of tungsten. Besides, as noted before, nonuniformities of this stripper are less detrimental than is the case for the BTA stripper due to the much smaller relative energy loss (0.02% as compared to 2.5%).

V. SUMMARY AND CONCLUSIONS

Following an extensive research and development effort, the old 24.2 mg/cm^2 thick graphite foil that strips 100 MeV/nucleon gold ions from charge 31^+ to charge 77^+ between the booster and the AGS was replaced by a thinner and more uniform stripper made of an optimized combination of 6.4 mg/cm^2 aluminum and 9.2 mg/cm^2 vitreous carbon. The stripper located between the AGS and RHIC that removes the last two electrons from 10 GeV/nucleon gold ions was also replaced. The old stripper was an Al_2O_3 plate having an effective thickness of 522 mg/cm^2, while the new one is made of 48.9 mg/cm^2 tungsten.

In Table III we summarize the results of these stripper improvements. The intensity losses in the BTA stripper are mainly due to the population of charge states other than 77^+. Nuclear fragmentation only plays a minor roll (0.4% for the old stripper and 0.2% for the new one).

The intensity losses in the ATR stripper are much reduced. The nuclear fragmentation loss is now 0.1% while it was 4% before. There is an incomplete stripping loss of $\sim$0.2% now, while this loss was less than 0.01% before.

The kinetic energy loss in the BTA stripper is reduced by $\sim 1/3$ while there is over a factor 15 reduction for the ATR stripper. The BTA energy loss reduction is however the more important one because the percent energy loss is larger and because its reduction alleviates the booster-AGS beam phase mismatch introduced by this stripper.

The measured longitudinal emittance growth reduction from a factor 4 to 1.8 for the BTA stripper is mainly due to better material uniformity. For the ATR stripper, the longitudinal emittance growth is also reduced, but it was already negligible with the old stripper. The transverse emittance growths for both strippers were also reduced, but they were already fairly small before.

The main operational advantages for gold acceleration achieved with the new strippers are primarily associated with an AGS longitudinal emittance reduction by a factor of $\sim$2 at extraction, and potentially larger in the future, and minimization of beam losses in the ATR stripper, leading to better efficiency and virtual elimination of associated activation concerns.

The reduced longitudinal emittance from the AGS and the possibility of another significant reduction may provide added incentive to preserve this emittance as well as possible during RHIC injection and ramping to minimize

TABLE III. Comparison of old and new BTA and ATR stripper performance.

Stripper	Intensity loss (%)	Kinetic energy loss (%)	Longitudinal emittance increase (%)	Rms angular scattering (μ radians)	Horizontal emittance increase (%)	Vertical emittance increase (%)
Old BTA	38	3.74	400	450	1.6	14.7
New BTA	36	2.45	180	410	1.3	12.4
Old ATR	4.0	0.35	0.1[a]	30	2.0	2.0
New ATR	0.3	0.02	0.06[b]	14	0.43	0.43

[a]Estimated from a 200 μ-inch stripper surface roughness measurement.
[b]Estimated assuming and upper limit of 10% tungsten foil thickness variation over the beam spot size.

future beam cooling times. To realize the additional AGS longitudinal emittance reduction, it may become necessary to mitigate or eliminate the gold ion velocity mismatch at AGS injection which can in principle be done either by an acceleration stage in the BTA line (~ 6 MV accelerating potential for charge 77^+) or by increasing the booster orbit radius by $\sim 1\%$. This last solution would require moving and realigning magnets and vacuum chambers around the ring and is probably not practical having also a deleterious effect on proton operations.

A third option being seriously considered is to use one special AGS accelerating cavity that has a very wide bandwidth to either follow the misphased bunches at injection and adiabatically move them to properly spaced buckets or to damp the synchrotron oscillations of the bunches created by the phase errors described above.

The beam diagnostic instrumentation used in this work allows measurements of sufficient precision to provide meaningful comparisons with model predictions based in some cases on considerable extrapolation. Reasonable qualitative agreement with the models shows that they are very useful to guide stripper performance optimization. Relatively small but systematic and significant measured discrepancies may aid in improving the models.

Reaching fully stripped heavy ions such as gold or lead is essential for their acceleration and especially for their storage at relativistic energies both because of the economy of magnetic accelerator lattices and because of vacuum requirements that would otherwise be practically unachievable. Independently of the charge states obtained from various types of ion sources and early acceleration stages, the last two stripping stages are likely to remain the same for future accelerators. (i) Stripping of all electrons but two, i.e. producing heliumlike ions can be exceptionally efficient ($\sim 64\%$ in our case) because of the relatively large binding energy of the K-electrons. (ii) Full stripping can be done essentially without losses at a sufficiently high energy where the electron loss cross sections exceed by far the electron capture cross sections, especially with strippers made of large atomic number elements.

The present improvements will thus hopefully benefit future relativistic heavy ion accelerators and our comparisons of measurements and predictions may help to further refine the models.

ACKNOWLEDGMENTS

We would like to thank Veljko Radeka for valuable advice and Rolf Beuttenmuller for careful and expert laser cutting of the vitreous carbon material. We are grateful to Chellis Chasman for interesting discussions on nuclear fragmentation. Finally, we thank the Tandem and Main Control Room operators for providing the beams used in the measurements, and for accumulating valuable operational information. This manuscript has been authored by employees of Brookhaven Science Associates, LLC under Contract No. DE-AC02-98CH10886 with the U.S. Department of Energy.

[1] R. Anholt, Phys. Rev. A **31**, 3579 (1985).
[2] H. Gould, D. Greiner, P. Lindstrom, T. J. M. Symons, H. Crawford, P. Thieberger, and H. E. Wegner, Nucl. Instrum. Methods Phys. Res., Sect. B **10**, 32 (1985).
[3] P. Thieberger, H. E. Wegner, J. Alonso, H. Gould, R. E. Anholt, and W. E. Meyerhof, IEEE Trans. Nucl. Sci. **32**, 1767 (1985).
[4] W. E. Meyerhof, R. Anholt, J. Eichler, H. Gould, Ch. Munger, J. Alonso, P. Thieberger, and H. E. Wegner, Phys. Rev. A **32**, 3291 (1985).
[5] R. Anholt, W. E. Meyerhof, H. Gould, Ch. Munger, J. Alonso, P. Thieberger, and H. E. Wegner, Phys. Rev. A **32**, 3302 (1985).
[6] W. E. Meyerhof, R. Anholt, Ziang-Yuan Xu, H. Gould, B. Feinberg, R. J. McDonald, H. E. Wegner, and P. Thieberger, Nucl. Instrum. Methods Phys. Res., Sect. A **262**, 10 (1987).
[7] R. Anholt, W. E. Meyerhof, X.-Y. Xu, H. Gould, B. Feinberg, R. J. McDonald, H. E. Wegner, and P. Thieberger, Phys. Rev. A **36**, 1586 (1987).
[8] W. E. Meyerhof, R. Anholt, X.-Y. Xu, H. Gould, B. Feinberg, R. J. McDonald, H. E. Wegner, and P. Thieberger, Phys. Rev. A **35**, 1967 (1987).
[9] R. Anholt, W. E. Meyerhof, X.-Y. Xu, Harvey Gould, B. Feinberg, R. J. McDonald, H. E. Wegner, and P. Thieberger, Phys. Rev. A **36**, 1586 (1987).

[10] H. P. Hülskötter, B. Feinberg, W. E. Meyerhof, A. Belkacem, J. R. Alonso, L. lumenfeld, E. A. Dillard, H. Gould, N. Guardala, G. F. Krebs, M. A. McMahan, M. E. Rhoades-Brown, B. S. Rude, J. Schweppe, D. W. Spooner, K. Street, P. Thieberger, and H. E. Wegner, Phys. Rev. A **44**, 1712 (1991).

[11] R. Anholt and W. E. Meyerhof, Phys. Rev. A **16**, 190 (1977).

[12] R. Anholt and W. E. Meyerhof, Phys. Rev. A **33**, 1556 (1986).

[13] W. E. Meyerhof, R. Anholt, J. Eichler, and A. Salop, Phys. Rev. A **17**, 108 (1978).

[14] R. Anholt, Ch. Stoller, J. D. Molitoris, D. W. Spooner, E. Morenzoni, S. A. Andriamonje, and W. E. Meyerhof, H. Bowman, J.-S. Xu, Z.-Z. Xu, J. O. Rasmussen, and D. H. H. Hoffmann, Phys. Rev. A **33**, 2270 (1986).

[15] R. Anholt and U. Becker, Phys. Rev. A **36**, 4628 (1987).

[16] W. E. Meyerhof, Phys. Rev. A **18**, 414 (1978).

[17] W. E. Meyerhof, R. Anholt, and Xiang-Yuan Xu, Phys. Rev. A **35**, 1055 (1987).

[18] Th. Stöhlker, H. Geissel, H. Folger, C. Kozhuharov, P. H. Mokler, G. Münzenberg, D. Scahardt, Th. Schawab, M. Steiner, H. Stelzer, and K. Sümmerer, Nucl. Instrum. Methods Phys. Res., Sect. B **61**, 408 (1991).

[19] C. Scheidenberger, H. Geissel, Th. Stöhlker, H. Folger, H. Irnich, C. Kozhuharov, H. Magel, P. H. Mokler, R. Moshammer, G. Münzenberg, F. Nickel, M. Pfützner, P. Rymuza, W. Schwab, J. Ulrich, B. Voss, Nucl. Instrum. Methods Phys. Res., Sect. B **90**, 36 (1994).

[20] Th. Stöhlker, C. Kozhuharov, P. H. Mokler, A. Warczak, F. Bosh, H. Geissel, R. Moshammer, C. Schidenberger, J. Eichler, A. Ichihara, T. Shirai, Z. Stachura, P. Rymuza, Phys. Rev. A **51**, 2098 (1995).

[21] Th. Stöhlker, D. C. Ionescu, P. Rymuza, F. Bosh, H. Geissel, C. Kozhuharov, T. Ludziejewsky, P. H. Mokler, C. Schidenberger, A. Warczak, and R. W. Dunford, Phys. Rev. A **57**, 845 (1998).

[22] C. Scheidenberger, Th. Stölker, W. E. Meyerhof, H. Gissel, P. H. Mokler, and B. Blank, Nucl. Instrum. Methods Phys. Res., Sect. B **142**, 441 (1998).

[23] O. B. Tarasov and D. Bazin, Nucl. Phys. **A746**, 411 (2004).

[24] GLOBAL and CHARGE codes accessible as utilities in LISE++, http://groups.nscl.msu.edu/lise/.

[25] T. Roser, 1993 Particle Accelerator Conference, p. 3207, http://accelconf.web.cern.ch/AccelConf/p93/PDF/PAC1993_3207.PDF.

[26] T. Roser, L. A. Ahrens, and H. C. Hseuh, EPAC 1994, p. 2441, http://accelconf.web.cern.ch/AccelConf/e94/PDF/EPAC1994_2441.PDF.

[27] Smolyakov, W. Fischer, C. Omet, and P. Spiller, GSI-Acc-Report-2005-11-001, 2005, BNL C-A/AP/117, 2006.

[28] L. Ahrens, J. Alessi, J. Benjamin, M. Blaskiewicz, J. M. Brennan, K. A. Brown, C. Carlson, W. Fischer, C. J. Gardner, J. W. Glenn, M. Harvey, T. Hayes, Haixin Huang, G. Marr, J. Morris, F. Pilat, T. Roser, F. Severino, K. S. Smith, D. Steski, P. Thieberger, N. Tsoupas, A. Zaltsman, and K. Zeno, PAC Proceedings, Albuquerque, NM, 2007.

[29] L. Ahrens, J. Benjamin, M. Blaskiewicz, J. M. Brennan, C. J. Gardner, H. C. Hseuh, Y. Y. Lee, R. K. Reece, T. Roser, A. Soukas, and P. Thieberger, IEEE Proceedings of the 1995 Particle Accelerator Conference, 1993, p. 378.

[30] http://www.srim.org/ and *The Stopping and Range of Ions in Solids*, edited by J. F. Ziegler, J. P. Biersack, and U. Littmark (Pergamon Press, New York, 1985).

[31] Graphite grade ZXF-5Q, 0.005 in. thick, fabricated by Poco Graphite, Inc., Decatur, Texas, U.S.A.

[32] G. Marr, L. Ahrens, P. Thieberger, and K. Zeno, Brookhaven National Laboratory C-A/AP/#124, 2003; L. Ahrens (private communication).

[33] Brand name SIGRADUR® K fabricated by HTW Hochtemperatur-Werkstoffe GmbH, Germany.

[34] C. Scheidenberger (private communication).

[35] H. Huang, W. Buxton, V. Castillo, J. W. Glenn, G. Mahler, M. Syphers, W. van Asselt, R. L. Witkover, and S. Y. Zhang, Proceedings PAC97, IEEE 1998, p. 2155; and http://www.princetonscientific.com/pp./harp.html.

[36] D. Gassner and R. Witkover, http://www.agsrhichome.bnl.gov/RHIC/Instrumentation/Systems/InjProfile/flags.html.

[37] D. B. Steski, J. Alessi, J. Benjamin, C. Carlson, M. Manni, P. Thieberger, and M. Wiplich, *Proceedings of PAC2001* (IEEE, New York, 2001), p. 2545.

[38] P. Maier-Komor, G. Dollinger, and H. J. Körner, Nucl. Instrum. Methods Phys. Res., Sect. A **438**, 73 (1999).